

Low-temperature magnetization of (Ga,Mn)As semiconductors

T. Jungwirth,^{1,2} J. Mašek,³ K.Y. Wang,² K.W. Edmonds,² M. Sawicki,⁴ M. Polini,⁵ Jairo Sinova,⁶ A.H. MacDonald,⁷ R.P. Campion,^{8,9} L.X. Zhao,^{8,9} N.R.S. Farley,^{8,9} T.K. Johal,⁹ G. van der Laan,⁹ C.T. Foxon,² and B.L. Gallagher²

¹*Institute of Physics ASCR, Cukrovarnická 10, 162 53 Praha 6, Czech Republic*

²*School of Physics and Astronomy, University of Nottingham, Nottingham NG7 2RD, UK*

³*Institute of Physics ASCR, Na Slovance 2, 182 21 Praha 8, Czech Republic*

⁴*Institute of Physics, Polish Academy of Sciences, 02668 Warszawa, Poland*

⁵*NEST-INFM and Scuola Normale Superiore, I-56126 Pisa, Italy*

⁶*Department of Physics, Texas A&M University, College Station, Texas 77843-4242, USA*

⁷*Department of Physics, University of Texas at Austin, Austin TX 78712-1081*

⁸*School of Physics and Astronomy, University of Nottingham, Nottingham NG7 2RD, United Kingdom*

⁹*CCLRC Daresbury Laboratory, Warrington WA4 4AD, United Kingdom*

We report on a comprehensive study of the ferromagnetic moment per Mn atom in (Ga,Mn)As ferromagnetic semiconductors. Theoretical discussion is based on microscopic calculations and on an effective model of Mn local moments antiferromagnetically coupled to valence band hole spins. The validity of the effective model over the range of doping studied is assessed by comparing with microscopic tight-binding/coherent-potential approximation calculations. Using the virtual crystal $k \cdot p$ model for hole states, we evaluate the zero-temperature mean-field contributions to the magnetization from the hole kinetic and exchange energies, and magnetization suppression due to quantum fluctuations of Mn moment orientations around their mean-field ground state values. Experimental low-temperature ferromagnetic moments per Mn are obtained by superconducting quantum interference device and x-ray magnetic circular dichroism measurements in a series of (Ga,Mn)As semiconductors with nominal Mn doping ranging from $\sim 2\%$ to 8%. Hall measurements in as-grown and annealed samples are used to estimate the number of uncompensated substitutional Mn moments. Based on our comparison between experiment and theory we conclude that all these Mn moments in high quality (Ga,Mn)As materials have nearly parallel ground state alignment.

PACS numbers: 75.50.Pp, 75.30.Gw, 73.61.Ey

I. INTRODUCTION

Early experimental studies of (Ga,Mn)As ferromagnetic semiconductors, reporting large apparent magnetization deficits,^{1,2} motivated a theoretical search for possible intrinsic origins of frustrating magnetic interactions in this material. Using a wide spectrum of computational techniques, ranging from *ab initio* LDA methods^{3,4} and microscopic tight-binding approximations⁵ to semiphenomenological, $k \cdot p$ kinetic-exchange models,^{6,7,8,9,10} the theoretical studies have identified several mechanisms that can lead to non-collinear ground states. The observation that long wavelength spin-waves with negative energies frequently occur within a spherically symmetric kinetic-exchange model illustrates⁶ that randomness in the distribution of Mn moments can result in an instability of the collinear ferromagnetic state. Frustration can be further enhanced when positional disorder is combined with anisotropies in Mn-Mn interactions. The *pd* character of electronic states forming the magnetic moment leads to magnetic interaction anisotropies with respect to the crystallographic orientation of the vector connecting two Mn moments.^{3,4,5,8} When spin-orbit coupling is taken into account,^{5,7,9,10} magnetic interactions also become anisotropic with respect to the relative orientation of the Mn-Mn connecting vector and the magnetic moment.

Some degree of non-collinearity is inevitable as a com-

bined consequence of positional disorder and spin-orbit coupling. Nevertheless a large suppression of the ferromagnetic moment is not expected theoretically⁵ in metallic (Ga,Mn)As samples with Mn concentrations above 1%. The minor role of non-collinearity is due largely to the long-range character of magnetic interactions, which tends to average out the frustrating effect of anisotropic coupling between randomly distributed Mn impurities. In this paper we present detailed calculations of zero temperature magnetization in (Ga,Mn)As ferromagnets and compare the results with superconducting quantum interference device (SQUID) and x-ray magnetic circular dichroism (XMCD) measurements in a series of samples with nominal Mn doping ranging from $\sim 2\%$ to 8%. Our calculations neglect effects that would lead to non-collinearity, appealing to expectations that these effects are small. Our assumption is consistent with experimental observations of larger ferromagnetic moments in recently synthesized high-quality samples.^{11,12} The substantial magnetization suppression seen in many early (Ga,Mn)As samples is attributed here primarily to the role played in those samples by interstitial Mn atoms. The consistency of the theoretical and experimental data that we are able to achieve, allows us to rule out any marked magnetic frustrations in the ground state of high-quality (Ga,Mn)As ferromagnets, and helps to clarify the character of magnetic interactions in this material.

Two distinct theoretical approaches are used in the paper to discuss magnetization in (Ga,Mn)As semiconduc-

tors. In the more microscopic approach we account explicitly for the five d -orbital electrons on a substitutional Mn_{Ga} impurity, and for the strong on-site Coulomb correlations that suppress spin and charge fluctuations of the $L = 0$, $S = 5/2$ state of the atomic Mn d -shell. Magnetism in the mixed crystal arises in this picture from electron hopping between the Mn d -states and p -orbitals concentrated on the As sublattice that form the top of the host semiconductor valence band. For weak $p-d$ hybridization, a second approach is possible. The Schrieffer-Wolff transformation¹³ allows us to map the microscopic Hamiltonian onto an effective Hamiltonian for local $S = 5/2$ moments and valence band states whose coupling is described by the kinetic-exchange term, $J_{pd}\hat{\mathbf{S}}(\mathbf{R}) \cdot \hat{\mathbf{s}}(\mathbf{r})\delta(\mathbf{R} - \mathbf{r})$, where $\hat{\mathbf{S}}$ and $\hat{\mathbf{s}}$ are the local moment and valence band state spin operators, respectively. This approach will fail if the $p-d$ hybridization is too strong, but appears to be reliable for (Ga,Mn)As.

The paper is organized as follows: In Section II we identify the key physical considerations related to ground-state magnetization of (Ga,Mn)As ferromagnets by focusing first on a single $\text{Mn}(d^5+\text{hole})$ complex. We recall the connection between $p-d$ hybridization and the antiferromagnetic kinetic-exchange coupling, digress on the sign of the hole contribution to total moment per Mn, and discuss the expected mean-field contribution to magnetization per Mn from the Mn local moment and from the antiferromagnetically coupled hole. We also explain that quantum fluctuations around the mean-field ground state are generically present because of antiferromagnetic character of the $p-d$ kinetic exchange interaction.

Magnetization calculations for the many-Mn-impurity system are discussed in Section III. The relevant considerations here parallel those that apply for isolated $\text{Mn}(d^5+\text{hole})$ complexes, but differ in detail because of interactions between moments. Zero temperature ferromagnetic moments per Mn are first studied within the tight-binding/coherent-potential approximation (TBA/CPA) model. The results of these microscopic calculations indicate that (Ga,Mn)As is in a weak $p-d$ hybridization regime over the whole range of Mn concentrations that we study. These calculations help establish theoretically the validity of the effective kinetic-exchange model. The virtual crystal approximation and the $\mathbf{k} \cdot \mathbf{p}$ effective Hamiltonian are then used to evaluate contributions to the mean-field magnetization from hole kinetic and exchange energies and to confirm the expected weak role quantum fluctuations around the mean-field many-body ground state.

Experimental SQUID and XMCD data are presented in Section IV. Partial concentrations of substitutional and interstitial Mn impurities and the corresponding number of uncompensated local moments are derived from the nominal Mn doping and from Hall measurements of the hole density in as-grown and annealed samples.¹² The collinearity of the ferromagnetic ground state in the (Ga,Mn)As materials we study is tested by

comparing experimental data with theoretical calculations. Section V briefly summarizes main conclusions of the paper.

II. MAGNETIZATION OF AN ISOLATED $\text{Mn}(d^5+\text{HOLE})$ COMPLEX

A. $d^5+\text{hole}$ picture

Most of the spectral weight near the top of the GaAs valence band originates from As $4p$ levels. Magnetic coupling between these states and the strongly localized $3d$ electrons on the substitutional Mn_{Ga} atom, which is at the origin of ferromagnetism in (Ga,Mn)As materials, is dominated by the $p-d$ hybridization contribution.¹⁴ The majority spin d -shell, with all five electron spins aligned forming a large spin $S = 5/2$, has its spectral weight centered ~ 3.5 eV below the top of the valence band. The empty, minority-spin d -level overlaps with the conduction band. Hybridization between p and d orbitals therefore, increases the energy of the majority-spin p orbitals (level repulsion) and favors the occupation of minority-spin p orbitals. This is the basic origin of the antiferromagnetic interaction represented by J_{pd} , as explained further in Fig. 1.

Apart from providing a magnetic moment, the substitutional Mn_{Ga} impurity acts as a moderately shallow single-acceptor in GaAs.¹⁵ The cartoon in top panel of Fig. 1 shows the splitting of the impurity level due to $p-d$ hybridization and the lower panel of Fig. 1 illustrates the many-Mn system in which the impurity level is broadened, eventually merging with the host valence band at higher Mn concentrations. To avoid confusion that may result from using the hole picture to describe magnetization of carriers in p-type (Ga,Mn)As materials, we make a digression here and explain the relation between magnetizations as evaluated using the physical electron-picture (as in Fig. 1) and magnetizations evaluated using the indirect but computationally more convenient hole-picture.

Magnetization at $T = 0$ is defined thermodynamically by the dependence of the ground-state energy E on external magnetic field B :

$$m = -\left.\frac{\partial E}{\partial B}\right|_{B=0} \quad (1)$$

In this paper we always assume $\mathbf{B} \parallel +\hat{z}$. In a mean-field picture the magnetization is related to the change of single-particle energy with field, summed over all occupied orbitals. Orbitals that decrease in energy with field make a positive contribution to the magnetization. For $\mathbf{B} \parallel +\hat{z}$, the d -electron spins are aligned along $-z$ -direction (down-spins) and the majority spin band electrons have spin-up due to antiferromagnetic $p-d$ exchange coupling. Then, if the majority spin band moves up in energy with B and the minority band moves down,

as illustrated in the left part of Fig. 2, the band kinetic energy increases with B and, according to Eq. (1), the corresponding contribution to the magnetization is negative. In the hole-picture, we obtain the same respective sense of shifts of the majority *hole* and minority *hole* bands, as illustrated in the right part of Fig. 2, and therefore the correct (negative in our case) sign of the magnetization. The cartoon shows that in order to circumvent the rather confusing notion of a spin of a hole in magnetization calculations, the full Hamiltonian $\hat{H}(B)$ should be derived in the physical electron picture where the sign of the coupling of the electron spin to B is unambiguously defined. The electron picture \rightarrow hole picture transformation ($\hat{H}(B) \rightarrow -\hat{H}(B)$) and the clearly defined notion of majority and minority bands in either picture guarantees the consistency in sign of the calculated magnetization. Note that the language used here neglects spin-orbit interactions which lead to single-particle orbitals that do not have definite spin character. Although spin-orbit interactions are important they can be neglected in most qualitative considerations, like the ones we explain here. In this paper we occasionally make statements which neglect spin-orbit interactions, and they should always be understood in this spirit.

The electron-electron exchange energy has a negative sign and its magnitude increases monotonically when moving from the paramagnetic to the half-metallic (empty minority band) state. This together with Eq. (1) implies that the magnetization contribution from the electron-electron exchange energy has the same sign as the contribution from the kinetic energy. Using the same arguments as above we see in the exchange energy case the sign of magnetization is also treated consistently in the electron picture \rightarrow hole picture transformation.

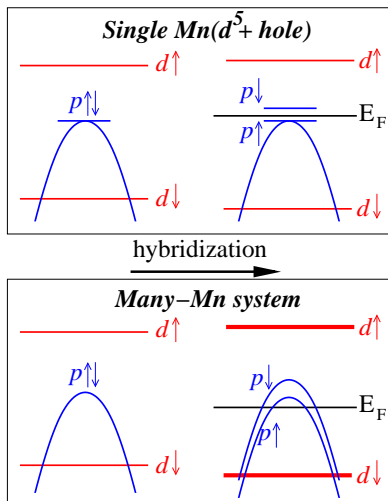


FIG. 1: Electron-picture cartoon: splitting of the isolated Mn acceptor level (top panel) and of the top of the valence-band in the many-Mn system (bottom panel) due to p-d hybridization.

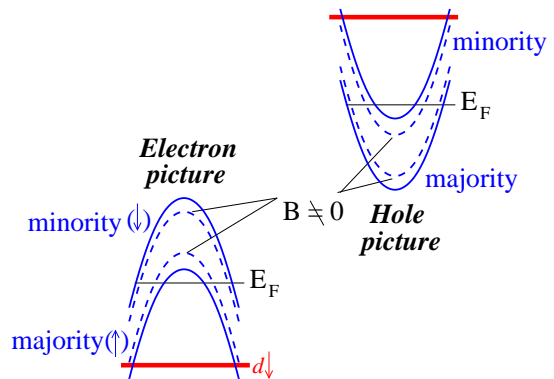


FIG. 2: Cartoon of Zeeman coupling of an external magnetic field assuming $g > 0$ in the electron and hole pictures for our valence band coupled to Mn moments system. Majority band in both electron and hole pictures moves up in energy resulting in a negative band-contribution to the magnetization.

B. Mean-field magnetization

In a model which for the many-Mn-impurity system corresponds to a mean-field approximation, the ground state wavefunction of the Mn(d^5 +hole) complex reads $|S_z = -S\rangle|j_z = +j\rangle$ and the magnetization per Mn equals $m_{MF} = (g_S S - g_j j)\mu_B$, where S and j are local d -electrons and hole moments and g_S and g_j are the respective Landé g-factors. The five d -electrons have zero total orbital angular momentum, i.e. $g_S = 2$, and for spin $j = 1/2$ hole ($g_j = 2$) we get $m_{MF} = 4\mu_B$. Hole states near the valence band edge have a p -character, however, so more realistically we should consider $g_j j = 4/3 * 3/2 = 2$ which gives $m_{MF} = 3\mu_B$. We show in the next section that this basic picture of a suppressed m_{MF} due to holes applies also to highly Mn-doped (Ga,Mn)As materials although the magnitude of the mean-field hole contribution is weaker because of the occupation of both majority and minority hole bands and, partly, because of spin-orbit coupling effects.

C. Quantum fluctuations contribution to magnetization

The two-spin, S and j model allows us also to readily demonstrate the presence of quantum fluctuations around the mean-field ground state, which is related to the antiferromagnetic sign of the $\mathbf{S} \cdot \mathbf{j}$ coupling. We show that for the Mn(d^5 +hole) complex, quantum fluctuations are expected to weakly suppress the mean-field magnetization m_{MF} . Detailed many-body calculations discussed in the following section confirm the role of quantum fluctuations is also weak for the many-Mn systems.

In the limit of $B \rightarrow 0$ we can write the two-spin Hamiltonian as,

$$\mathcal{H} = J \hat{\mathbf{S}} \cdot \hat{\mathbf{j}} = \frac{J}{2} (\hat{S}_{tot}^2 - \hat{S}^2 - \hat{j}^2), \quad (2)$$

where $\hat{S}_{tot} = \hat{S} + \hat{j}$. For comparison we first consider ferromagnetic coupling, $J < 0$. Since in this case $S_{tot} = S + j$, the ground-state eigenenergy, $E_{FM} = -\frac{|J|}{2}[(S + s)(S + j + 1) - S(S + 1) - j(j + 1)] = -|J|Sj$, equals to the mean-field energy, i.e., the mean-field state is exact. For ferromagnetic $\mathbf{S} \cdot \mathbf{j}$ coupling, the quantum fluctuation contribution to the magnetization is strictly absent in the many-Mn case only when the hole system is half-metallic (*i.e.* when the minority band is empty). We can see this by introducing spin raising and lowering operators in the Hamiltonian (2),

$$\mathcal{H} = J \left[\hat{S}_z \hat{j}_z + \frac{1}{2} (\hat{S}^+ \hat{j}^- + \hat{S}^- \hat{j}^+) \right]. \quad (3)$$

Quantum fluctuations are absent when the transverse spin terms above annihilate the many-particle ground state. When acting on a state with all localized spins *and* all band spins polarized in the same direction, both transverse terms produce zero. For partially spin-polarized bands, quantum fluctuation corrections, although not strictly zero, are qualitatively smaller than in the antiferromagnetic case.

For antiferromagnetic coupling ($J > 0$), $S_{tot} = S - j$ and the corresponding ground-state energy $E_{AF} = \frac{|J|}{2}[(S - j)(S - j + 1) - S(S + 1) - j(j + 1)] = -|J|(Sj + j)$ is lower than the mean-field energy. The mean-field ground state is not exact here and quantum fluctuation corrections to the magnetization will be non-zero in general. To estimate the correction we write the exact ground-state wavefunction as,

$$\begin{aligned} |\psi\rangle &= |S_{tot} = S - j, S_{tot,z} = -(S - j)\rangle \\ &= \sqrt{\frac{S}{S + j}} |S_z = -S, j_z = +j\rangle \\ &\quad - \sqrt{\frac{j}{S + j}} |S_z = -S + 1, j_z = +j - 1\rangle, \quad (4) \end{aligned}$$

the mean-field wavefunction as, $|\psi\rangle_{MF} = |S_z = -S, j_z = +j\rangle$, and evaluate the respective expectation values of the Zeeman Hamiltonian, $g_S \mu_B B \hat{S}_z + g_j \mu_B B \hat{j}_z$. From Eq. (1) we then obtain that the difference between the exact and mean-field state magnetizations is given by

$$m - m_{MF} \equiv m_{QF} = -\mu_B \frac{j}{S + j} (g_S - g_j). \quad (5)$$

When $j = 1/2$ and $g_S = g_j = 2$ the quantum fluctuation correction to the magnetization vanishes even though the mean-field ground state is not exact. The quantum fluctuation correction to the magnetization remains relatively weak also even when we adopt the more realistic description of the valence-band hole moment ($j = 3/2$, $g_j = 4/3$), for which $m_{QF} = -0.25\mu_B$.

III. MAGNETIZATION OF MANY-Mn-IMPURITY SYSTEM

A. Moments per Mn in the microscopic TBA/CPA model

The TBA description of (Ga,Mn)As mixed crystals is particularly useful for explaining the complementary role of local and itinerant moments in this p-type magnetic semiconductor. The language that is used to describe this interplay can differ depending on whether a fully microscopic or a kinetic-exchange model is employed, and this difference has sometimes led to confusion. This section represents an attempt at clarity. At the same time we find that the TBA/CPA results help establish the validity of the antiferromagnetic $p-d$ kinetic-exchange model and of the virtual crystal approximation for describing collinear ground states in highly doped (Ga,Mn)As ferromagnets.^{12,16}

In the TBA/CPA calculations, the hole density is varied independently of Mn doping by adding non-magnetic donors (Si or Se) or acceptors (C or Be). The d -electron magnetic moments of all Mn atoms are aligned along $+z$ -axis. The parameterization of the TBA Hamiltonian was chosen to provide the correct band gap for a pure GaAs crystal¹⁷ and the appropriate exchange splitting of the Mn d -states. Local changes of the crystal potential at Mn, represented by shifted atomic levels, were estimated using Ref. 18. Spin-orbit coupling is not included in our TBA Hamiltonian. In the CPA, disorder effects appear in the finite spectral width of hole quasiparticle states. The TBA/CPA technique can, therefore, capture changes in the $p-d$ interaction with doping due to both chemical alloying effects and positional disorder. In Fig. 3 we show the microscopic TBA/CPA magnetic moments per Mn, m_{TBA} , in $\text{Ga}_{1-x}\text{Mn}_x\text{As}$ ferromagnets plotted as a function of the hole density p relative to the Mn concentration $N_{Mn} = 4x/a_{lc}^3$ (a_{lc} is the semiconductor host lattice constant). The m_{TBA} is obtained here using the electron picture by integrating over occupied states up to the Fermi energy.

A common way of microscopically separating contributions from local atomic and itinerant moments is by projecting the occupied electron states onto Mn d -orbitals and sp -orbitals, respectively. In this decomposition, the resulting local Mn moments are smaller than $5\mu_B$ per Mn due to the admixture of d -character in empty states near the valence band edge. The effective kinetic-exchange model employed in the following sections corresponds, however, to a different decomposition of contributions, in effect associating one spectral region with local Mn moments and a different spectral region with itinerant hole moments. The kinetic-exchange model, in which local moments have $S = 5/2$, is obtained from the microscopic TBA/CPA model by expressing the total TBA/CPA moment as the difference between a contribution m_{TBA}^{int} resulting from integrating over all electronic states up to mid-gap, *i.e.* including the entire valence band, and a

contribution corresponding to the integral from Fermi energy to mid-gap. As long as the valence-conduction band gap is non-zero, the former contribution is independent of valence band filling and equals to the moment of an isolated Mn atom, $5\mu_B$. The latter term represents magnetization of itinerant holes.

The applicability of the effective kinetic-exchange model relies implicitly on the perturbative character of the microscopic $p-d$ hybridization. The level of the $p-d$ hybridization over the studied doping range is illustrated in Fig. 4 where we show the orbital composition of m_{TBA}^{int} . The filled symbols correspond to including spectral weights from all spd orbitals while the half-open and open symbols are obtained after projecting onto the d and sp orbitals, respectively. If no hybridization was present, then m_{TBA}^{int} projected on the d -orbitals would equal to the total m_{TBA}^{int} and the sp -orbital projected m_{TBA}^{int} would vanish. In our TBA/CPA calculations, the d -orbital projected m_{TBA}^{int} is reduced by only 10% as compared to the total m_{TBA}^{int} and, therefore, the $p-d$ hybridization can be regarded as a weak perturbation. The nearly constant value of the d -orbital projected m_{TBA}^{int} also suggests that the kinetic-exchange coupling parameter J_{pd} in the effective spin Hamiltonian is nearly independent of doping over the whole range of Mn and hole densities that we study.

The decrease of m_{TBA} in Fig. 3 with increasing p/N_{Mn} clearly demonstrates antiferromagnetic $p-d$ coupling over the whole range of dopings. The initial common slope for data corresponding to different Mn concentrations reflects the half-metallic nature of the hole system (only majority hole band occupied) when spin-orbit interactions are neglected. Here the hole contribution to magnetization per volume is proportional to p , i.e., magnetization per Mn is proportional to p/N_{Mn} . The change in the slope of m_{TBA} at larger hole densities, which now becomes Mn-density dependent, reflects population of the minority-spin hole band and, therefore, the additional dependence of hole magnetization on exchange splitting between majority- and minority-hole bands. In this regime the hole magnetization per volume is approximately proportional to pN_{Mn} , i.e., a common trend for different Mn densities is obtained when m_{TBA} is plotted versus p rather than p/N_{Mn} .

Within the TBA/CPA model, m_{TBA} corresponds to the total magnetization per Mn measured by a SQUID and we therefore expect these experimental values to lie between 4 and $5\mu_B$ and to increase with decreasing number of holes in collinear (Ga,Mn)As ferromagnets. The XMCD data on the other hand reflect local and d-state projected contribution from Mn and should be compared with the half-open symbols in Fig. 4, showing a negligible dependence on the hole density. These trends are indeed confirmed in our experiments. Before discussing the experimental data we refine, quantitatively, the above theoretical predictions for the total magnetization. For example, we expect that the number of minority holes at a given total hole density is underestimated in our TBA

model. This is caused in part by the quantitative value of the exchange spin-splitting of the valence band in the TBA/CPA calculations which is a factor of 1.5-2 larger than value inferred from experiment. Also since SO coupling is not included in our TBA model, we obtain three majority bands that are degenerate at the Γ -point, instead of only two bands (heavy- and light-hole) as in the more realistic SO-coupled band structure. (This substantial deficiency is common to all calculations that neglect spin-orbit coupling.) In addition to the underestimate of the minority hole density, the TBA/CPA calculations also omit the reduction of the mean spin-density in the majority band caused by the SO-coupling and, therefore, the total TBA magnetization values are too small. In the following section we attempt to correct for these quantitative shortcomings of the TBA calculations by taking the experimentally measured^{19,20} value of the $p-d$ coupling constant, $J_{pd} = 54 \pm 9$ meV nm³, and by evaluating valence band spin-splitting and SO coupling effects within the semiphenomenological $k \cdot p$ kinetic-exchange model.^{21,22} The weak dependence of the TBA/CPA valence band splitting on positional disorder justifies our use of the virtual crystal approximation in this semiphenomenological modeling of collinear (Ga,Mn)As ground states.

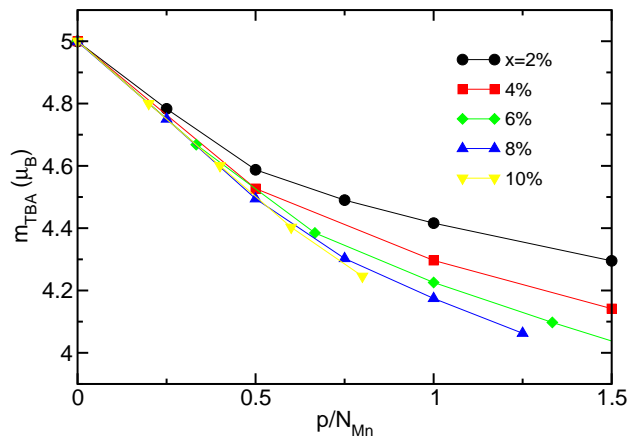


FIG. 3: Mean-field total magnetization per Mn as a function of hole density relative to the local Mn moment density. Results are obtained using the TBA/CPA model.

B. Mean-field magnetization contributions from hole kinetic and exchange energies

Within the semiphenomenological virtual crystal model the valence band holes experience a mean-field, $h_{MF} = J_{pd}N_{Mn}\langle S \rangle$, and the band Hamiltonian can then be written as, $\hat{H}_{MF} = \hat{H}_{KL}(B) + h_{MF}\hat{s}_z$, where $\hat{H}_{KL}(B)$

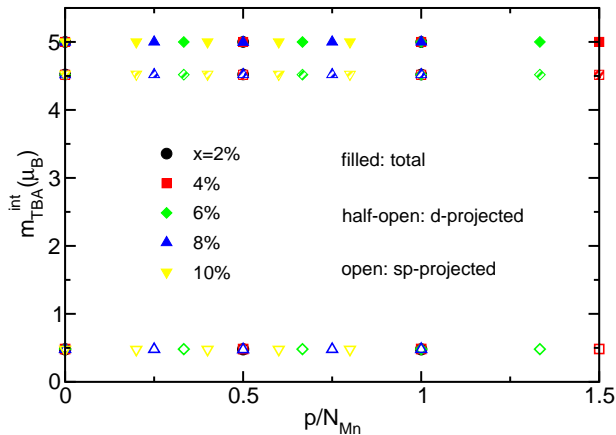


FIG. 4: Integrated total and d - and pd -projected magnetizations per Mn as a function of hole density relative to the local Mn moment density. See text for definition of m_{TBA}^{int} .

is the B -dependent six-band Kohn-Luttinger Hamiltonian of the GaAs host band^{22,23}, \hat{s}_z is the z -component of the hole spin operator, and $\langle S \rangle$ is the mean spin polarization of the local Mn moments.^{21,22,24} At $T = 0$, $\langle S \rangle = 5/2$ and the local moment contribution to the magnetization per Mn is $5\mu_B$. As emphasized above, this finding is *not* in contradiction with the smaller d -electron contribution to the magnetic moment in microscopic calculations.

Because of the SO interaction, both orbital and Zeeman couplings of the external magnetic field have to be included in $\hat{H}_{KL}(B)$. The SO-coupling and heavy-hole – light-hole mixing at finite wavevectors lead to magnetizations that cannot be expressed using a constant, Mn- and hole-density independent g -factor. Instead the kinetic band energy contribution to MF magnetization per Mn, m_{MF}^{kin} , is obtained by numerically integrating over all occupied hole eigenstates of \hat{H}_{MF} and by finding the coefficient linear in B of this kinetic energy contribution to the total energy.²² Results for several typical Mn dopings and hole densities are shown in Fig. 5. They agree quantitatively with earlier calculations reported in Ref. 22. As anticipated in Section II, m_{MF}^{kin} is negative, *i.e.* it suppresses the total magnetic moment. The magnitude of the hole MF magnetization per hole, $|m_{MF}^{kin}|N_{Mn}/p$, is smaller than $2\mu_B$ due to occupation of both majority and minority heavy- and light-hole bands at these typical (Ga,Mn)As hole densities (see inset of Fig. 5). In this case, as also emphasized in Section II, m_{MF}^{kin} is expected to fall into a common trend for different Mn densities when plotted against p . Data shown in the main panel of Fig. 5 confirm this expectation and indicate a ~ 0.2 to $0.4\mu_B$ suppression of the MF moment per Mn due to the hole kinetic energy contribution to magnetization.²²

To estimate the hole exchange energy contribution to magnetization per Mn, m_{MF}^{ex} , we use an expression of

the total exchange energy derived in the absence of SO-coupling and assuming spin-up and spin-down heavy-hole bands with effective mass $0.5m_e$,

$$E_{ex} = 2^{1/3} \frac{E_{ex}^P(n)}{p^{4/3}} \left[p_{\uparrow}^{4/3}(B) + p_{\downarrow}^{4/3}(B) \right], \quad (6)$$

where $p_{\uparrow(\downarrow)}$ is the density of the majority(minority) band, $p_{\uparrow} + p_{\downarrow} = p$, and the exchange energy of the paramagnetic state is given by

$$E_{ex}^P(n) = -\frac{e^2}{4\pi\epsilon} \frac{3}{4} \left(\frac{3}{\pi} \right)^{1/3} p^{4/3}. \quad (7)$$

The B -dependent hole densities can be written as

$$p_{\uparrow}(B) = p_{\uparrow}(0) - |g_j \mu_B B j| \frac{2G^{\uparrow} G^{\downarrow}}{G^{\uparrow} + G^{\downarrow}}$$

$$p_{\downarrow}(B) = p_{\downarrow}(0) + |g_j \mu_B B j| \frac{2G^{\uparrow} G^{\downarrow}}{G^{\uparrow} + G^{\downarrow}}, \quad (8)$$

where $G^{\uparrow(\downarrow)}$ is the density of states at the Fermi energy of the majority(minority) band. Combining Eqs. (6)-(8) and Eq. (1) we obtain

$$m_{MF}^{ex} = \frac{4}{3} \frac{2^{1/3}}{p^{4/3}} E_{ex}^P(n) g_j \mu_B j \frac{2G^{\uparrow} G^{\downarrow}}{G^{\uparrow} + G^{\downarrow}} \left(p_{\uparrow}(0)^{1/3} - p_{\downarrow}(0)^{1/3} \right). \quad (9)$$

In Fig. 6 we plot m_{MF}^{ex} values calculated assuming spin-1/2 holes, *i.e.* $g_j j = 1$. This contribution to the total MF magnetization is again negative, is nearly independent of x and p within the range of doping considered, and its magnitude is about a factor of 10 smaller than the magnitude of the term originating from the hole kinetic band energy. A more realistic estimate of m_{MF}^{ex} can be obtained by using $g_j j = g_{fit} * 3/2$ in Eq. (9). Here g_{fit} follows from fitting the m_{MF}^{kin} calculated within the parabolic heavy-hole band model to the full six-band numerical results in Fig. 5. The values of g_{fit} as a function of x and p are plotted in Fig. 7. These are similar to the $g_{j=3/2} = 4/3$ value that follows from the local atomic model and, therefore, m_{MF}^{ex} calculated from Eq. (9) using $g_j j = g_{fit} * 3/2$ is approximately a factor of 2 larger than m_{MF}^{ex} calculated assuming spin-1/2 holes. Combining all these considerations we conclude that the zero-temperature magnetization per Mn in the MF kinetic-exchange model has a positive contribution equal to $5\mu_B$ from the Mn local moments and a negative contribution from band holes which suppresses the moment per Mn by ~ 5 -10%.

C. Quantum fluctuation contribution to the magnetization

In Section II we argued that quantum fluctuation corrections to the isolated Mn d^5 -hole complex magnetization should be small. Here we demonstrate that this conclusion also applies to the many-Mn system.

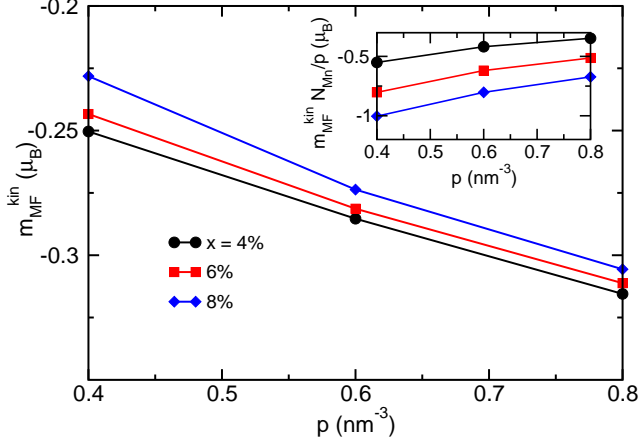


FIG. 5: Mean-field kinetic energy contribution to the hole magnetization per Mn as a function of hole density. These results were obtained using the six-band Kohn-Luttinger parameterization of the valence band and the kinetic-exchange model.

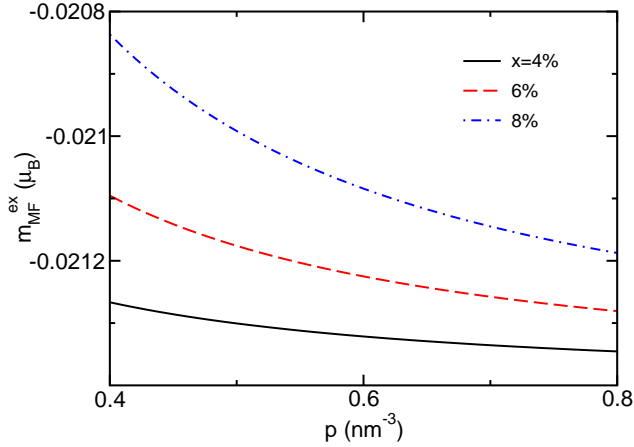


FIG. 6: Mean-field hole-hole exchange energy contribution to the hole magnetization per Mn as a function of hole density. These results were obtained using the spin-1/2, $m^* = 0.5m_e$ parabolic band kinetic-exchange model.

In these calculations we use the virtual crystal kinetic-exchange model and assume spin-1/2 heavy-holes with no SO-coupling and with the parabolic band dispersion ($m^* = 0.5m_e$). The many-body Hamiltonian of the

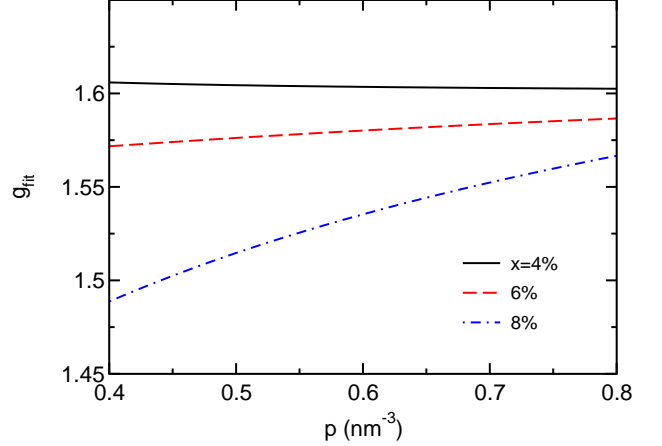


FIG. 7: Effective hole Landé g-factor obtained by fitting the kinetic energy term in hole magnetization calculated with the parabolic band kinetic-exchange model with $j = 3/2$ and $m^* = 0.5m_e$ to the numerical results of the six-band Kohn-Luttinger model from Fig. 5

model reads

$$\begin{aligned} \hat{H} = & \int d^3r \left[\sum_{\sigma} \hat{\Psi}_{\sigma}^{\dagger}(\vec{r}) \left(-\frac{\hbar^2 \nabla^2}{2m^*} - \mu \right) \hat{\Psi}_{\sigma}(\vec{r}) + g_j \mu_B \vec{B} \cdot \vec{j}(\vec{r}) \right. \\ & \left. + |J_{pd}| \sum_I \vec{S}(\vec{R}_I) \cdot \vec{j}(\vec{r}) \delta(\vec{r} - \vec{R}_I) \right] \\ & + g_S \mu_B \sum_I \vec{B} \cdot \vec{S}(\vec{R}_I). \end{aligned} \quad (10)$$

The imaginary time path-integral formulation of quantum statistical physics combined with a Holstein-Primakoff bosonic representation for the Mn local moments allows²⁵ us to formally express the free energy of interacting local and itinerant spins in terms of a path integral over coherent state labels \bar{z}, z :

$$\mathcal{Z} = \int \mathcal{D}(\bar{z}z) \exp(-S_{\text{eff}}[\bar{z}z]). \quad (11)$$

The effective action S_{eff} in Eq. (11) is obtained by integrating out fermionic (hole) degrees of freedom in Eq. (10). In the Gaussian fluctuation approximation²⁵

$$S_{\text{eff}}[\bar{z}z] = \frac{1}{\beta} \sum_m \int_{|\mathbf{q}| \leq q_c} \frac{d^3\mathbf{q}}{(2\pi)^3} \bar{z}(\mathbf{q}, \nu_m) D^{-1}(\mathbf{q}, i\nu_m) z(\mathbf{q}, \nu_m). \quad (12)$$

Here the inverse of the spin-wave propagator $D(\mathbf{q}, \nu_m)$ is given by

$$D^{-1}(\mathbf{q}, i\nu_m) = -i\nu_m + \varepsilon_{sw}(B) + \Sigma_{sw}(\mathbf{q}, i\nu_m, B), \quad (13)$$

$q_c = (6\pi^2 N_{Mn})^{1/3}$ is a Debye cutoff which ensures that we include the correct number of local-moment degrees

of freedom and

$$\varepsilon_{sw}(B) = -g_S \mu_B B + \frac{|J_{pd}|}{2} (p_{\uparrow}(B) - p_{\downarrow}(B)) \quad (14)$$

is the mean-field local moment spin-flip energy. The frequency-dependent self-energy $\Sigma_{sw}(\mathbf{q}, i\Omega, B)$ in Eq. (13) is given by

$$\Sigma_{sw}(\mathbf{q}, i\Omega, B) = \frac{N_{Mn} J_{pd}^2 S}{2} \times \int \frac{d^3\mathbf{k}}{(2\pi)^3} \frac{f(\varepsilon_{\mathbf{k}} - \mu + \Delta(B)/2) - f(\varepsilon_{\mathbf{k}+\mathbf{q}} - \mu - \Delta(B)/2)}{i\Omega + \varepsilon_{\mathbf{k}} - \varepsilon_{\mathbf{k}+\mathbf{q}} + \Delta(B)},$$

with $\varepsilon_{\mathbf{k}} = \hbar^2 k^2 / 2m^*$ and

$$\Delta(B) = N_{Mn} |J_{pd}| S - g_j \mu_B B. \quad (15)$$

The translational and rotational invariance of our model implies that $\Sigma_{sw}(\mathbf{q}, i\Omega)$ depends only of $|\mathbf{q}|$. The functional integration in Eq. (11) can be performed exactly using Eq. (12),

$$\mathcal{Z} = \frac{1}{\beta} \prod_{n, |\mathbf{q}| \leq q_c} \frac{1}{-i\nu_n + \varepsilon_{sw}(B) + \Sigma_{sw}(q, i\nu_n, B)}. \quad (16)$$

The quantum fluctuation correction to the free energy then reads,

$$\delta F_{QF} \equiv F - F_0 = -\frac{1}{\beta} \ln \frac{\mathcal{Z}}{\mathcal{Z}_0}, \quad (17)$$

where \mathcal{Z}_0 is given by Eq. (16) with the fluctuations term, $\Sigma_{sw}(q, i\nu_n, B)$, set to zero.

In Fig. 8 we plot the quantum fluctuations contribution to the magnetization per Mn obtained from

$$m_{QF} = - \left. \frac{\partial \delta E_{QF}}{\partial B} \right|_{B=0}. \quad (18)$$

As expected m_{QF} is small in the many-Mn system and we can conclude that quantum fluctuations lead to a $\sim 1\%$ suppression of the MF moment per Mn.

IV. EXPERIMENTAL DATA

A. Sample growth and preparation

In the theoretical sections of this paper we evaluated the zero-temperature magnetization per Mn in (Ga,Mn)As ferromagnets, using approximation schemes that would fail if the true ground state magnetization was highly non-collinear. We will now show that these theoretical results are consistent with low temperature magnetometry and XMCD experiments. A series of (Ga,Mn)As films with Mn content varying between 1.7-6.7% in the SQUID experiments and between 2.2 and 8.4% in the XMCD experiments were grown by low-temperature molecular beam epitaxy (MBE) using

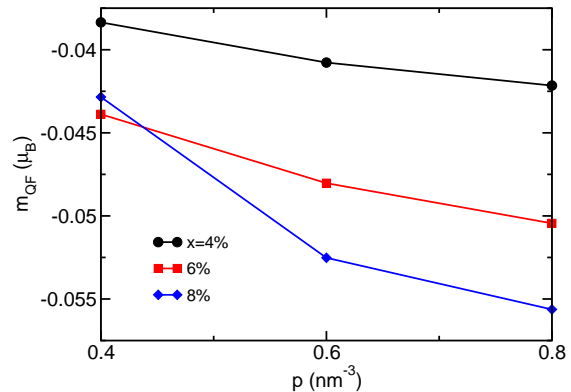


FIG. 8: Quantum fluctuation contribution to magnetization per Mn as a function of hole density. These results were obtained using the spin-1/2, $m^* = 0.5m_e$ parabolic band kinetic-exchange model.

As₂. The layer structure of the thin films consists of 25 or 50nm (Ga,Mn)As / 50nm low temperature GaAs / 100nm high temperature (580°C) GaAs / SI-GaAs(100) substrate. The growth temperature of the (Ga,Mn)As layer and the GaAs buffer was 180-300°C, decreasing with increasing Mn concentration in order to minimize As antisite densities while maintaining two-dimensional growth and preventing phase segregation. Further details on the growth are presented elsewhere.^{26,27}

The Mn concentrations were deduced from the in-situ measured Mn/Ga incident flux ratio, which was calibrated using secondary ion mass spectrometry (SIMS) measurements on 1 μm thick (Ga,Mn)As films, grown under otherwise identical conditions to the samples considered here. A detailed comparison of the results of a number of different calibration techniques, presented in detail elsewhere,²⁸ allows us to assign an uncertainty of 10% to the quoted total Mn doping, x . The SIMS measurements yield no information on the lattice site of the incorporated Mn, and we expect that Mn will be incorporated either on interstitial Mn_I or on substitutional Mn_{Ga} sites.²⁹ Post-growth annealing of the samples is performed in air at 190°C for 50-150 hours, which is an established procedure for removal of Mn_I from the (Ga,Mn)As layer. Curie temperatures in the as-grown materials are within the range of 40-80 K and in the annealed samples between 40 and 150 K.¹²

B. Magnetometry

The magnetic moment of the samples is measured in a SQUID magnetometer, at 5K and under a 0.3T external magnetic field. The external field is necessary to overcome in-plane anisotropy fields, so that the magnetization is aligned with the measurement axis of the SQUID.

The diamagnetic contribution from the substrate is subtracted. Measured magnetic moments normalized to the total Mn concentration as obtained from SIMS calibration, m_{SQUID} , are shown in Fig. 9. The moment decreases with increasing Mn concentration, and increases on annealing, similar to earlier reports.² This is consistent with the anticipated formation of interstitial Mn for doping above $\sim 2\%$,¹² given the antiferromagnetic coupling between Mn_I and Mn_{Ga} ,³⁰ and with breaking of this coupling by low-temperature annealing.^{29,31}

In order to compare the experimental data with the theoretical results of previous sections we have to replot the measured magnetizations as a function of the density of uncompensated Mn_{Ga} local moments, x_{eff} . To do this we need to determine the densities of substitutional Mn_{Ga} and interstitial Mn_I , x_s and x_i , in our (Ga,Mn)As materials. Given these values, we assume¹² that each Mn_I present in the system is antiferromagnetically coupled to one Mn_{Ga} and that both should be excluded from the active Mn fraction for comparison between theory and experiment, *i.e.* that $x_{eff} = x_s - x_i$.

To obtain the individual Mn impurity concentrations we rely on Hall effect and magnetoresistance measurements at high magnetic field (up to 16.5T) and low temperatures (down to 0.3K), from which we evaluate the experimental hole density p , after using a fitting procedure to separate normal and anomalous contributions to the Hall resistance.³² We then assume that the single acceptors Mn_{Ga} and double donors Mn_I are the only impurities that contribute to p , *i.e.*, $p = (4/a_{lc}^3)(x_s - 2x_i)$. From this expression and from the total Mn concentration obtained by SIMS calibration ($x = x_s + x_i$) we can estimate x_{eff} for both as-grown and annealed samples. A detailed discussion of the uncertainties associated with this procedure is given elsewhere.¹² The magnetic moment per effective Mn moment density, m_{SQUID}^{eff} , is shown in Fig. 10 as a function of p/N_{Mn}^{eff} where $N_{Mn}^{eff} = (4x_{eff}/a_{lc}^3)$. In agreement with the predictions of the theory section, m_{SQUID}^{eff} falls within the range $4-5\mu_B$ for all samples studied. Furthermore, although there is appreciable scatter, it can be seen that samples with lower hole densities tend to show higher m_{SQUID}^{eff} , consistent with a negative contribution to magnetization from antiferromagnetically coupled band holes.

C. X-ray Magnetic Circular Dichroism

XMCD measurements were performed using $(99 \pm 1)\%$ circular polarized x-rays from beamline ID8 at the European Synchrotron Radiation Facility. The samples are briefly etched in concentrated HCl prior to the measurements in order to remove Mn oxide rich surface layers, which may obscure the signal from the (Ga,Mn)As due to the relatively short probing depth of the measurement.³³ After etching, total electron yield and fluorescent yield measurements are in quantitative agreement, indicating

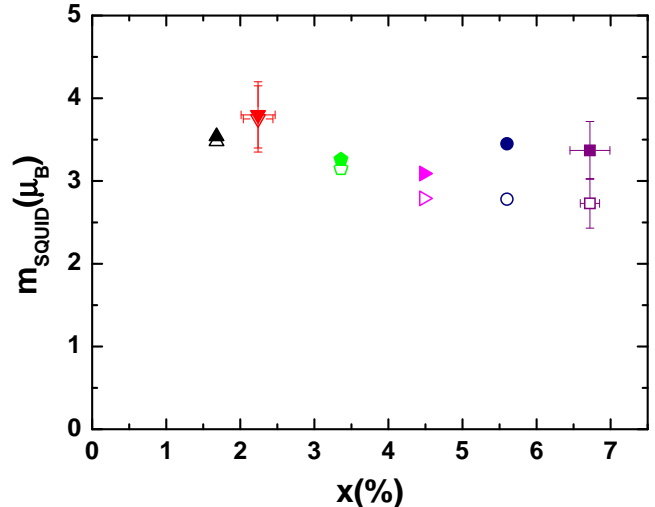


FIG. 9: SQUID magnetization per nominal total Mn density in as-grown (open symbols) and annealed (filled symbols) (Ga,Mn)As materials plotted as a function of the nominal Mn doping.

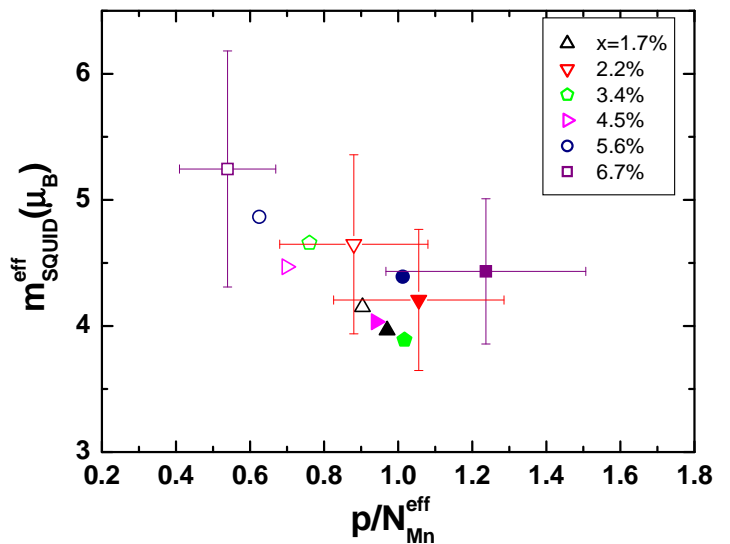


FIG. 10: SQUID magnetization per effective density of uncompensated Mn_{Ga} local moments in as-grown (open symbols) and annealed (filled symbols) (Ga,Mn)As materials plotted as a function of hole density per effective density of uncompensated Mn_{Ga} local moments.

a uniform distribution of Mn.

Fig. 11 shows Mn $L_{3,2}$ x-ray absorption spectra for an annealed (Ga,Mn)As sample with $x = 8.4\%$, for parallel and antiparallel orientations of the external magnetic field and the x-ray helicity vector. The sample temperature is 6K, and the external magnetic field is $\pm 1T$, ap-

plied perpendicular to the surface of the sample. A very large change in the absorption is observed on reversing the external field, with an asymmetry (difference to sum ratio) of up to 55% at the $L_{3,2}$ peak. $L_{3,2}$ absorption corresponds to transitions from the $2p$ core states to the unfilled $3d$ states, so the Mn $L_{3,2}$ spectra gives direct information on the polarization of the Mn $3d$ band. Applying the XMCD sum rules to the spectra allows quantitative and separate determination of the Mn $3d$ ground state orbital and spin magnetic moments.³⁴ The moments are obtained on a per atom basis, without requiring separate measurement of the Mn concentration, by normalizing to summed absorption signal. There are, however, inherent uncertainties in the application of the sum rules, in particular due to mixing of the $2p_{3/2}$ and $2p_{1/2}$ states which prevents the separate integration over each of the spin-orbit split core levels. Comparison of calculated spectra with their corresponding ground state moments reveals that a correction factor of 1.47 is required for the spin moment to account for this mixing. The Mn $3d$ moments obtained from XMCD are shown in Table I, for two annealed samples with low and high Mn doping. In both cases, magnetic moments of around $4.5\mu_B$ are obtained, in agreement with the SQUID results. Moreover, the measured moment and the property that it is independent of Mn doping is in very good agreement with the calculated d -projected magnetic moment shown in the inset of Fig. 4. We note here that the calculations shown in Fig. 4 account only for the spin angular momentum contribution to magnetization since SO-coupling effects were neglected in the TBA/CPA calculations.

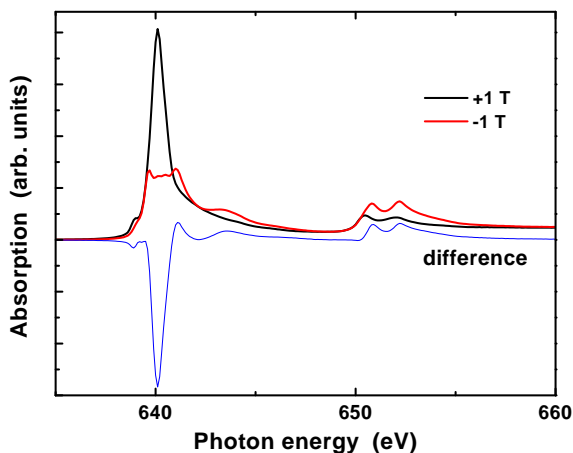


FIG. 11: Mn $L_{3,2}$ x-ray absorption spectra for an annealed (Ga,Mn)As sample with nominal Mn doping 8.4%, for parallel and antiparallel orientations of the external magnetic field and the x-ray helicity vector. The blue line shows the difference between the two spectra.

x (%)	m_{XMCD}^{spin} ($\pm 0.3\mu_B$)	m_{XMCD}^{orb} ($\pm 0.03\mu_B$)	$m_{XMCD}^{spin} + m_{XMCD}^{orb}$ ($\pm 0.3\mu_B$)
2.2	4.3	0.15	4.5
8.4	4.3	0.16	4.5

TABLE I: Mn $3d$ moments obtained from XMCD and decomposed into the spin and orbital contributions in annealed samples with nominal Mn doping 2.2 and 8.4%.

V. CONCLUSIONS

We report on a combined theoretical and experimental analysis of the spontaneous magnetization in (Ga,Mn)As diluted magnetic semiconductor ferromagnets. We find that the thermodynamic magnetization is dominated by a large local moment contribution of $5\mu_B$ from nearly collinear substitutional Mn atoms. Evaluation of the smaller magnetization contribution from the valence band system that couples the local moments together involves a number of subtleties. In this paper we included hole-hole exchange interactions and we also accounted for spin-orbit coupling which means that no valence band orbital is completely spin-polarized and which substantially changes the overall electronic structure. Quantum fluctuations of the band and local moment orientations also play a role because of the antiferromagnetic interaction between band and local moment spins. The end result of all these corrections is a magnetization per magnetically active Mn ion that is suppressed from $5\mu_B$ by $\sim 5 - 10\%$. Comparison with experimental data can be made reliably only after accounting for the formation of interstitial Mn complexes during the MBE growth, and for their subsequent removal by post-growth annealing. Once these corrections have been applied, we find, within the experimental error bars, agreement between theory and experiment. The interpretation of XMCD magnetization measurements, which capture only the d -electron contribution, requires a recognition of the hybridized p - d character of both local moment and band-electron contributions to the magnetization. Comparison of these measurements with TBA/CPA calculations provides experimental support for the applicability of the kinetic-exchange model in (Ga,Mn)As ferromagnets. Finally, our combined theoretical and experimental work demonstrates that non-collinearity does not play a significant role in the magnetization of high-quality metallic (Ga,Mn)As ferromagnets.

Acknowledgment

We thank Julio Cesare, Peter Bencok and Nick Brookes for their contributions to the XMCD experiment. This work was supported by the Grant Agency of the Czech Republic through Grant No. 202/05/0575, by the Academy of Sciences of the Czech Republic through Institutional Support No. AV0Z10100521, by the EU FENIKS project EC:G5RD-CT-2001-00535, by the UK

EPSRC through Grant GR/S81407/01, by the Welch Foundation, and the US Department of Energy under

grant DE-FG03-02ER45958.

-
- ¹ H. Ohno and F. Matsukura, *Solid State Commun.* **117**, 179 (2001).
- ² S. J. Potashnik, K. C. Ku, R. Mahendiran, S. H. Chun, R. F. Wang, N. Samarth, and P. Schiffer, *Phys. Rev. B* **66**, 012408 (2002).
- ³ P. Mahadevan, A. Zunger, and D. Sarma, *Phys. Rev. Lett.* **93**, 177201 (2004).
- ⁴ J. Kudrnovský, I. Turek, V. Drchal, F. Máca, P. Weinberger, and P. Bruno, *Phys. Rev. B* **69**, 115208 (2004).
- ⁵ C. Timm and A. MacDonald, *Phys. Rev. B* **71**, 155206 (2005).
- ⁶ J. Schliemann and A. MacDonald, *Phys. Rev. Lett.* **88**, 137201 (2002).
- ⁷ J. Schliemann, *Phys. Rev. B* **67**, 045202 (2003).
- ⁸ L. Brey and G. Gómez-Santos, *Phys. Rev. B* **68**, 115206 (2003).
- ⁹ G. Zaránd and B. Jankó, *Phys. Rev. Lett.* **89**, 047201 (2002).
- ¹⁰ G. A. Fiete, G. Zaránd, B. Jankó, P. Redliński, and C. P. Moca, *Phys. Rev. B* **71**, 115202 (2005).
- ¹¹ K. W. Edmonds, N. R. S. Farley, T. K. Johal, G. van der Laan, R. P. Champion, B. L. Gallagher, and C. T. Foxon, *Phys. Rev. B* **71**, 064418 (2005).
- ¹² T. Jungwirth, K. Wang, J. Mašek, K. Edmonds, J. König, J. Sinova, M. Polini, N. Goncharuk, A. MacDonald, M. Sawicki, et al., *cond-mat/0505215*.
- ¹³ J. R. Schrieffer and P. A. Wolff, *Phys. Rev.* **149**, 491 (1966).
- ¹⁴ A. K. Bhattacharjee, G. Fishman, and B. Coqblin, *Physica B+C* **117-118**, 449 (1983).
- ¹⁵ M. Linnarsson, E. Janzén, B. Monemar, M. Kleverman, and A. Thilderkvist, *Phys. Rev. B* **55**, 6938 (1997).
- ¹⁶ T. Jungwirth, J. Mašek, J. Sinova, and A. MacDonald, *Phys. Rev. B* **68**, 161202(R) (2003).
- ¹⁷ D. N. Talwar and C. S. Ting, *Phys. Rev. B* **25**, 2660 (1982).
- ¹⁸ W. Harrison, *Electronic Structure and the Properties of Solids* (Freeman, San Francisco, 1980).
- ¹⁹ J. Okabayashi, A. Kimura, O. Rader, T. Mizokawa, A. Fujimori, T. Hayashi, and M. Tanaka, *Phys. Rev. B* **58**, R4211 (1998).
- ²⁰ T. Omiya, F. Matsukura, T. Dietl, Y. Ohno, T. Sakon, M. Motokawa, and H. Ohno, *Physica E* **7**, 976 (2000).
- ²¹ M. Abolfath, T. Jungwirth, J. Brum, and A. MacDonald, *Phys. Rev. B* **63**, 054418 (2001).
- ²² T. Dietl, H. Ohno, and F. Matsukura, *Phys. Rev. B* **63**, 195205 (2001).
- ²³ I. Vurgaftman, J. Meyer, and L. Ram-Mohan, *J. Appl. Phys.* **89**, 5815 (2001).
- ²⁴ T. Dietl, H. Ohno, F. Matsukura, J. Cibert, and D. Ferrand, *Science* **287**, 1019 (2000).
- ²⁵ J. König, T. Jungwirth, and A. MacDonald, *Phys. Rev. B* **64**, 184423 (2001).
- ²⁶ R. Champion, K. Edmonds, L. Zhao, K. Wang, C. Foxon, B. Gallagher, and C. Staddon, *J. Cryst. Growth* **247**, 42 (2003).
- ²⁷ C. T. Foxon, R. P. Champion, K. W. Edmonds, L. Zhao, K. Wang, N. R. S. Farley, C. R. Staddon, and B. L. Gallagher, *J. Mater. Sci.* **15**, 727 (2004).
- ²⁸ L. X. Zhao, R. P. Champion, P. F. Fewster, R. W. Martin, B. Y. Ber, A. P. Kovarsky, C. R. Staddon, K. Y. Wang, K. W. Edmonds, C. T. Foxon, et al., *Semicond. Sci. Technol.* **20**, 369 (2005).
- ²⁹ K. M. Yu, W. Walukiewicz, T. Wojtowicz, I. Kuryliszyn, X. Liu, Y. Sasaki, and J. K. Furdyna, *Phys. Rev. B* **65**, 201303 (2002).
- ³⁰ J. Blinowski and P. Kacman, *Phys. Rev. B* **67**, 121204 (2003).
- ³¹ K. Edmonds, P. Boguslawski, K. Wang, R. Champion, N. Farley, B. Gallagher, C. Foxon, M. Sawicki, T. Dietl, M. Nardelli, et al., *Phys. Rev. Lett.* **92**, 037201 (2004).
- ³² K. W. Edmonds, R. P. Champion, K.-Y. Wang, A. C. Neumann, B. L. Gallagher, C. T. Foxon, and P. C. Main, *J. Appl. Phys.* **93**, 6787 (2003).
- ³³ K. W. Edmonds, N. R. S. Farley, R. P. Champion, C. T. Foxon, B. L. Gallagher, T. K. Johal, G. van der Laan, M. MacKenzie, J. N. Chapman, and E. Arenholz, *Appl. Phys. Lett.* **84**, 4065 (2004).
- ³⁴ P. Carra, B. T. Thole, M. Altarelli, and X. Wang, *Phys. Rev. Lett.* **70**, 694 (1993).